Characterization of Copy Number Variations in Oral Cavity Squamous Cell Carcinoma Reveals a Novel Role for MLLT3 in Cell Invasiveness

Chun-I Wang,[a,†] Huang-Kai Kao,[b,d,†] Ting-Wen Chen,[f,g,h] Yenlin Huang,[c] Hsing-Wen Cheng,[a] Jui-Shan Yi,[a,e] Shao-Yu Hung,[b] Chi-Sheng Wu,[a,e] Yun-Shien Lee,[i] Kai-Ping Chang[a,d,e]

[a]Department of Otolaryngology–Head and Neck Surgery, [b]Department of Plastic and Reconstructive Surgery, and [c]Department of Pathology, Chang Gung Memorial Hospital, Taoyuan, Taiwan; [d]College of Medicine and [e]Molecular Medicine Research Center, Chang Gung University, Taoyuan, Taiwan; [f]Institute of Bioinformatics and Systems Biology, [g]Biological Science and Technology, and [h]Center for Intelligent Drug Systems and Smart Bio-devices (IDS[2]B), National Chiao Tung University, Hsinchu, Taiwan; [i]Department of Biotechnology, Ming-Chuan University, Taoyuan, Taiwan
[†]Contributed equally.
Disclosures of potential conflicts of interest may be found at the end of this article.

Key Words. Copy number variations • Oral cavity squamous cell carcinoma • MLLT3 • CITED4 • HIF-1α

Abstract

Background. DNA copy number variations (CNVs) are a hallmark of cancer, and the current study aimed to demonstrate the profile of the CNVs for oral cavity squamous cell carcinoma (OSCC) and elucidate the clinicopathological associations and molecular mechanisms of a potential marker derived from CNVs, mixed-lineage leukemia translocated to chromosome 3 protein (MLLT3), in OSCC carcinogenesis.

Materials and Methods. CNVs in 37 OSCC tissue specimens were analyzed using a high-resolution microarray, the OncoScan array. Gene expression was analyzed by real-time polymerase chain reaction in 127 OSCC and normal tissue samples. Cell function assays included cell cycle, migration, invasion and chromatin immunoprecipitation assays.

Results. We found a novel copy number amplified region, chromosome 9p, encompassing MLLT3 via the comparison of our data set with six other OSCC genome-wide CNV data sets. MLLT3 overexpression was associated with

poorer overall survival in patients with OSCC (*p* = .048). MLLT3 knockdown reduced cell migration and invasion. The reduced invasion ability in MLLT3-knockdown cells was rescued with double knockdown of MLLT3 and CBP/ p300-interacting transactivator with ED rich carboxy-terminal domain 4 (CITED4; 21.0% vs. 61.5%). Knockdown of MLLT3 impaired disruptor of telomeric silencing-1-like (Dot1L)-associated hypermethylation in the promoter of the tumor suppressor, CITED4 (*p* < .001), and hence dysregulated HIF-1α-mediated genes (*TWIST*, *MMP1*, *MMP2*, *VIM*, and *CDH1*) in OSCC cells.

Conclusion. We identified unique CNVs in tumors of Taiwanese patients with OSCC. Notably, MLLT3 overexpression is related to the poorer prognosis of patients with OSCC and is required for Dot1L-mediated transcriptional repression of CITED4, leading to dysregulation of HIF-1α-mediated genes. *The Oncologist* 2019;24:e1388–e1400

Implications for Practice: This article reports unique copy number variations in oral cavity squamous cell carcinoma (OSCC) tumors of Taiwanese patients. Notably, MLLT3 overexpression is related to the poorer prognosis of patients with OSCC and is required for Dot1L-mediated transcriptional repression of CITED4, leading to dysregulation of HIF-1α-mediated genes.

Introduction

Oral cavity squamous cell carcinoma (OSCC) is one of the most common malignant diseases, accounting for more than 10,000 deaths every year and approximately 3% of all cancer cases estimated annually worldwide [1, 2]. Although there have been improvements in therapeutic approaches, the 5-year overall survival rate of patients with OSCC remains at

approximately 50% [3, 4]. Environmental risk factors, including cigarette smoking, alcohol consumption, and betel quid chewing, contribute to the development and progression of OSCC by facilitating genetic changes, genomic aberrations, and widespread genomic instability [5–7]. The contemporary treatment is mainly based on tumor staging and include surgery and adjuvant therapies, such as chemotherapy and radiotherapy. Although the improvement of the current diagnostic and therapeutic strategies, the 5-year overall survival rate has still been approximately 60% for last few decades [4]. In order to improve the detection and/or treatment of OSCC, the discovery of OSCC-associated biomarkers may increase our understanding of the OSCC tumorigenesis and disclose the associated molecular mechanisms.

Genetic factors play an important role in the etiology of OSCC, and the development and progression of OSCC result from a multistep pathway involving an accumulation of genetic alterations in proto-oncogenes and tumor suppressor genes for carcinogenesis, including chromosomal alterations, DNA copy number variations (CNVs; amplifications and deletions), and epigenetic alterations [8–10]. Detecting carcinogenetic abnormalities in OSCC might provide an important prognostic indicator of patient prognosis and contribute to tailored treatment for specific markers in the future. CNVs are a hallmark of cancer that may lead to oncogene activation and/or tumor suppressor gene inactivation in several malignancies, and they are important for understanding the mechanisms of disease and identifying clinical biomarkers, such as recurrence risk and response to therapy [11, 12]. Previously, Salahshourifar et al. compared 12 studies that used array comparative genomic hybridization on OSCC tumors and found common genomic CNVs and their frequency. The results indicated that the progression of oral premalignant lesions to invasive carcinomas involved a sequential accumulation of genetic changes. Furthermore, the accumulation of genetic changes increased in disease progression and in accordance with frequency, type, and extent of the abnormalities, even on different regions of the same chromosome. By the comparison, the researchers found that the amplifications on 3q (36.5%), 5p (23%), 7p (21%), 8q (47%), 11q (45%), and 20q (31%) and the deletions on 3p (37%), 8p (18%), 9p (10%), and 18q (11%) were the most common CNV regions among those studies [13]. These previous investigations support the theory that genomic alterations could be used as diagnosis and/or prognostic factors and as therapeutic targets in cancer.

To demonstrate the profile of the genetic alterations in OSCC, we applied a high-resolution microarray, OncoScan FFPE Express 2.0 System (OncoScan array), for determining the CNVs from 37 formalin-fixed paraffin-embedded (FFPE) tissue specimens in Taiwanese patients with OSCC (OSCC-Taiwan). The genomics platform is ideally suited to the use of FFPE samples for analysis of CNVs, as the requirement of input DNA is less than 80 ng and this platform can utilize extremely degraded DNA, with probes having a genomic footprint of just 40 bp [14]. Using this strategy, frequent CNVs were observed, and a novel copy number amplified region was identified in OSCC. From our CNV analyses, we found that mixed-lineage leukemia (MLL) translocated to chromosome 3 protein (MLLT3/AF9) is a promising biomarker in the Taiwanese population.

MLLT3 is a proline- and serine-rich protein of 568 amino acids that contains a KKRKK (amino acids 296–300) nuclear localization sequence; these features are typical of many transcription factors. MLLT3 was first identified as one of the 60 fusion partners of the MLL gene in acute leukemia that results from translocations at the 11q23 locus [15, 16]. MLLT3 protein interacts with many different factors and has been implicated in different cellular processes [17, 18]. In the extensive network of interacting proteins, MLLT3 has been reported to be associated with disruptor of telomeric silencing-1-like (Dot1L) [19, 20], the main enzyme responsible for histone H3 lysine 79 (H3K79) methylation [21–23]. Dot1L is implicated in UV damage repair [24] and affects gene expression in yeast, flies, and mammals [25, 26], whereas H3K79 methylation is involved in activation [27] and suppression [28] of several genes. Following this line, MLLT3-Dot1L complexes mediate transcriptional activation through increased levels of dimethylated H3K79 at the Hoxa9 promoter [27] but are also capable of transcriptional repression through hypermethylation of H3K79 at the ENaCα and Tbr1 promoter [19, 29]. In tumorigenesis, MLLT3 mediates transcriptional activation and was classified as a proto-oncogene via binding to the transcriptional repressor BCL-6 corepressor [30]. However, the function of MLLT3 in OSCC cells has not yet been elucidated.

Herein, we used an OncoScan array to detect frequent CNVs in OSCC. We compared our data set with previous genome-wide CNV data sets, and we found and validated a novel CNV region, 9p. From this finding, we subsequently identified a novel oncogene, *MLLT3*, in OSCC carcinogenesis. Accordingly, in the current study, we aimed to elucidate the clinicopathological associations and molecular mechanisms of MLLT3 in OSCC cells.

MATERIALS AND METHODS

Patient Populations and Clinical Specimens

Written informed consent was acquired from all of the patients enrolled in this study before sample collection, and this study was approved by the Institutional Review Board of Chang Gung Memorial Hospital, Taoyuan, Taiwan. Patients whose untreated OSCC tumors were primarily managed by surgical resection and who did not receive radiation or chemotherapy prior to surgery were enrolled in the study. Patients with at least one of the following conditions were considered ineligible and excluded from the study: the occurrence of synchronous or metachronous primary cancer, death from unnatural causes (such as suicide), and failure to receive adjuvant therapy when indicated. The FFPE OSCC specimens for OncoScan analysis were obtained from one training cohort, including 37 samples, and the clinicopathological features of the cases are summarized in supplemental online Table 1. Tumor specimens and pericancerous normal tissues for real-time quantitative polymerase chain reaction (PCR) analysis were obtained from another two testing cohorts, including 8 and 127 patients that were surgically resected and enrolled consecutively among the patients diagnosed with OSCC from 2006 to 2013. The patients in this study underwent standard preoperative assessments according to the institutional guidelines, including a detailed medical history, complete

physical examination, computed tomography or magnetic resonance imaging scans of the head and neck, chest radiographs, bone scans, and abdominal ultrasounds. Primary tumors were excised with adequate margins under intraoperative frozen section control. After surgery, pathological TNM classification of all tumors was performed according to the American Joint Committee on Cancer Staging Manual (2010). After discharge, all patients had regular follow-up visits every 2 months for the first year, every 3 months for the second year, and every 6 months thereafter.

DNA Extraction, FFPE Sample Gene Chip Analysis, and Analysis of Molecular Inversion Probe Data

First, 10-μm FFPE samples were sliced, and the tumor area was marked by pathologists on a hematoxylin- and eosin-stained slide. Samples with surface areas of 100 mm^2 were prepared for DNA extraction. Using the QIAamp DNA FFPE Tissue Kit (Qiagen, Germantown, MD), tissue sections were deparaffinized, and DNA was extracted and eluted for quality and quantity inspection according to the manufacturer's instructions. DNA concentration and purity were determined using the Qubit Fluorometer (Thermo Fisher Scientific, Waltham, MA). The extracted samples were further processed at the Genomic Medicine Research Core laboratory in Chang Gung Memorial Hospital at Linkou for OncoScan FFPE platforms to analyze copy number variations [31, 32]. The data of the molecular inversion probe and the percentage of the genome that changed were analyzed by using SNP-FASST2 in Nexus Express software version 3.1 (BioDiscovery, El Segundo, CA). The SNP-FASST2 algorithm was used for the segmentation and calling of chromosomal amplification and deletion with the following default parameters: significance threshold, 1.0E-8; maximal contiguous probe spacing, 1,000 Kbp; minimal number of probes per segment, 3; amplification, 0.1; and deletion, −0.15. Chromosomal amplifications or deletions smaller than 1.5 Mb were filtered. There was a total of 875 genes in the OncoScan gene chip targeting tumor suppressor genes or oncogenes; each gene had 20–40 probes depending on the length of the gene. The percentage of the genome that changed showed the number of aberrations for each patient divided by the total of 875 genes. The frequent CNV regions were determined using following criteria: the CNV frequency was more than 20% in 37 samples, and the chromosome regions contained more than two CNV genes. Accordingly, supplemental online Tables 2 and 3 show frequent copy number amplified or deleted regions, respectively, encompassing genes.

CNV and Relationship Analysis Between MLLT3 and Other Genes in OSCC Data from The Cancer Genome Atlas

CNV analysis of OSCC data from The Cancer Genome Atlas (TCGA) was performed as we have previously described [33]. Briefly, level 3 RNASeqV2 data for head and neck squamous cell carcinoma (HNSCC) were downloaded from TCGA [34] together with their clinical information. A total of 315 unique OSCC samples, whose anatomic sites and histopathological characteristics were identified as being within the oral cavity and as squamous cell carcinoma, respectively, were used in this analysis. Among the 315 patients, only 314 had available information for Kaplan-Meier plotting and survival analyses.

Spearman's correlation between the expression levels of MLLT3 and all the other genes were calculated with Partek Genomics Suite software, followed by adjustment of the p value with the Benjamini-Hochberg method. Using a p value less than .05 as cutoff value, we identified 434 genes that were inversely correlated with MLLT3 in the OSCC data set from TCGA (OSCC-TCGA).

Cell Culture

OEC-M1 cells were maintained in Roswell Park Memorial Institute medium 1640 (Thermo Fisher Scientific) containing 10% fetal bovine serum (FBS) plus antibiotics; OC3 cells were cultured at a 1:2 ratio in Dulbecco's modified Eagle's medium containing 10% FBS and keratinocyte serum-free medium (Thermo Fisher Scientific) plus antibiotics. The cells were cultured at 37°C in a humidified atmosphere of 95% air and 5% CO_2.

Gene Knockdown of MLLT3 and CITED4 Using Small Interfering RNA

Briefly, 19-nucleotide RNA duplexes targeting human MLLT3 or CBP/p300-interacting transactivator with ED rich carboxy-terminal domain 4 (CITED4) were synthesized and annealed by Dharmacon (Thermo Fisher Scientific). OEC-M1 and OC3 cells were transfected with the Dharmacon ON-TARGETplus Non-targeting Control Pool (Thermo Fisher Scientific), which contained pool of four small interfering RNAs (siRNAs) designed and tested for minimal targeting of human, mouse, or rat genes or MLLT3-pooled siRNA (GAACCUAAACCCAUGUCAA, UCUAAGUCGUUGAGGGAAU, GCAAAUAAAGAAUGGUGAA, and AGGCAUACCUAGAUGAACU) or CITED4-pooled siRNA (ACGCCG AACUCAUCGACGA, GGCCAGAGCGAGUUCGACU, CCUCGGCCG UAAAGUGAAA, and CCAAAAUAAAACUGGGUCA) using Lipofectamine RNAiMAX reagents (Thermo Fisher Scientific) according to the manufacturer's protocol. After 48 hours' transfection, cell lysates were prepared for Western blotting to determine gene knockdown efficacy.

RNA Extraction and Quantitative Reverse Transcription Polymerase Chain Reaction

OSCC tumor and normal counterpart tissues were homogenized in liquid nitrogen with a mortar and pestle and incubated with RNAzol B reagent (Tel-Test, Friendswood, TX). The RNA was further purified using an RNeasy cleanup kit (Qiagen) according to the manufacturer's protocol. First-strand cDNA was synthesized from 5 μg of total RNA and then mixed with a reaction mixture consisting of commercially available primers (TP63 Hs00978340_m1, EXT1 Hs00609162_m1, MEN1 Hs003 65720_m1, MITF Hs01117294_m1, MLH1 Hs00979919_m1, LPL Hs00173425_m1, MLLT3 Hs00971092_m1 and normalization control B2M, Hs00984230_m1; Assay-on-Demand, Thermo Fisher Scientific), RNase-free water, and TaqMan Universal PCR Master Mix. Real-time quantitative PCR (qPCR) was performed and analyzed using a 7900 HT Sequence Detection System and SDS version 2 (Applied Biosystems). All experiments were repeated in duplicate.

Flow Cytometry Analysis

Cells transfected with control siRNA or MLLT3 siRNA for 48 hours were harvested by trypsinization. For cell cycle analysis, cells were fixed in 70% ice-cold ethanol comprising

2 mg/mL RNase for 30 minutes and ultimately stained with propidium iodide (PI; 50 mg/mL) for 10 minutes. The fluorescence of PI in control siRNA or MLLT3 siRNA-transfected cells was determined using flow cytometry analysis (FACScan System, Becton Dickinson, San Diego, CA). We counted the percentage of cells in the G0/G1, S, and G2/M phases using CellQuest programs.

Cell Migration and Invasion Assay

OC3 and OEC-M1 cells were transfected with control siRNA or indicated siRNA for 48 hours. After transfection, the cells were harvested by trypsinization and suspended in serum-free culture medium. For the migration assay, the cells (300 µl; 5 × 104 cells) were added to the upper chambers of 24-well Transwell plates (0.8-µm pore size filter; Corning, Canton, NY), and each lower chamber was filled with 600 µl of serum-free culture medium containing 10 µl/mL fibronectin. After a 6-hour incubation at 37°C, the chambers were gently washed twice with phosphate-buffered saline and fixed with 100% methanol for 15 minutes, followed by Giemsa staining. The observer was blinded to the experimental condition, and these cells were counted for nine different fields of middle region per filter (around 70% coverage per filter) using an inverted microscope (Carl Zeiss, Oberkochen, Germany) equipped with a × 20 objective, followed by quantification using ImageJ software. For the invasion assay, the upper chambers of 24-well Transwell plates were coated with Matrigel Basement Membrane Matrix (BD Biosciences, San Jose, CA) at 37°C for 2 hours. The cells (1 × 105 cells) were suspended in 200 µl of serum-free culture medium and added to the upper chamber; each lower chamber was filled with 600 µl of serum-free culture medium. After a 16-hour incubation at 37°C, the chambers were washed, fixed, stained, and counted as described above.

Chromatin Immunoprecipitation Assay

Chromatin immunoprecipitations (ChIPs) were performed using ChIP-IT Express Enzymatic Magnetic Chromatin Immunoprecipitation kit according to the manufacturer's instructions (Active Motif, Carlsbad, CA). Briefly, cells transfected with control siRNA or MLLT3 siRNA for 24 hours were cross-linked with 1% formaldehyde for 10 minutes, followed by stop using glycine stop fix solution. Cells were scraped with lysis buffer provided with the kit and transferred cells to an ice-cold Dounce homogenizer, and broke the cells on ice with ten strokes to obtain the isolated nuclei. Isolated nuclei were then subjected to enzymatic digestion using enzymatic shearing cocktail for 15 minutes. The DNA fragments obtained ranged between 200 and 1,000 bp. Chromatin fractions were immunoprecipitated with Dot1L antibodies (Abcam, Cambridge, MA), and IgG (Santa Cruz Biotechnology, Dallas, TX) as a control. Cross-linking was reversed, and the proteins were removed by proteinase K treatment. DNA samples were analyzed by qPCR with the primer surrounding the transcriptional start site (TSS; +1) of the human *CITED4* gene (forward primer, CCACCGCGCGCTGTCCC; reverse primer, CGGCGGA CGGCGGCCTC) and *TCF4* gene (forward primer, TTCCAAAATTG CTGCTGGT; reverse primer, CGTCTTTGAAGGAAATCAGT). The experimental background was determined by performing a control ChIP with a nonspecific IgG. The averages of the

background signals for primer pairs were similar and are graphically represented by the dotted line.

Statistical Analysis

The Wilcoxon test was used to analyze the qPCR result from OSCC and normal counterpart tissues. The results of flow cytometry, migration, and invasion assays and mRNA expression in the OSCC cell lines were analyzed using the nonparametric Mann-Whitney U test. Chi-square tests were used to determine the differences between the MLLT3 expression and various clinicopathologic factors. Two-tailed p values of .05 or less were considered significant. A comparison of survival rates was carried out using the Kaplan-Meier method examined by the log-rank test. Statistical analyses were performed using SAS software (version 9.3; SAS Institute, Cary, NC). All patients underwent follow-up evaluations at our outpatient clinic until December 2016 or death.

RESULTS

CNV Landscape for OSCC-Taiwan

To uncover genomic alterations that could prove useful as molecular markers for OSCC tumors, a total of 37 patients with OSCC were included in the study. All of the above samples were analyzed using OncoScan array with subsequent data analysis using Nexus version 3.1. The 37 samples that applied for OncoScan analysis were further categorized on the basis of CNVs and percent genome (Fig. 1A). Our findings (OSCC-Taiwan) largely recapitulated the profile found in OSCC-TCGA (Fig. 1B), which included significantly amplified/deleted regions encompassing genes such as *TP63, EGFR, EXT1, FANCG, MEN1, PCNA, MITF, MLH1, FGFR1, LPL*, and *CSMD1.* In summary, our analysis demonstrated frequent copy number amplifications on chromosomes 3q, 5p, 7p, 8q, 9p, 9q, 11q, 14q, 17q, 20p, and 20q, encompassing 106 genes (Fig. 1A and supplemental online Table 2), and deletions on 3p and 8p, encompassing 46 genes (Fig. 1A and supplemental online Table 3). Information about each patient's risk factors is presented in Figure 1C. In addition, we verified six genes in the most frequent CNV regions that had been reported in previous study [13], including three copy number amplified genes (*TP63* in chromosome 3q, *EXT1* in chromosome 8q, and *MEN1* in chromosome 11q) and three copy number deleted genes (*MITF* in chromosome 3p, *MLH1* in chromosome 3p, and *LPL* in chromosome 8p) by real-time qPCR analysis, with a view to determining the mRNA levels in first testing cohort, including eight OSCC tissue specimens containing tumors and their corresponding normal tissues. As shown in Figure 1D, the mRNA levels of the two copy number amplified genes, *TP63* and *EXT1*, were higher in OSCC tumor tissues (p = .0274 and .0244, respectively) compared with those of normal counterpart tissues. The mRNA levels of the two copy number deleted genes, *MITF* and *LPL*, were lower in OSCC tumor tissues (p = .0016 and .0003, respectively) compared with those of the corresponding normal tissues. On the other hand, although the mRNA levels of *MEN1* and *MLH1* were not significantly different between OSCC tumor and normal counterpart tissues (p = .1723 and .1645, respectively), the results and the trends shown are still quite consistent with the consensus that CNV is one of
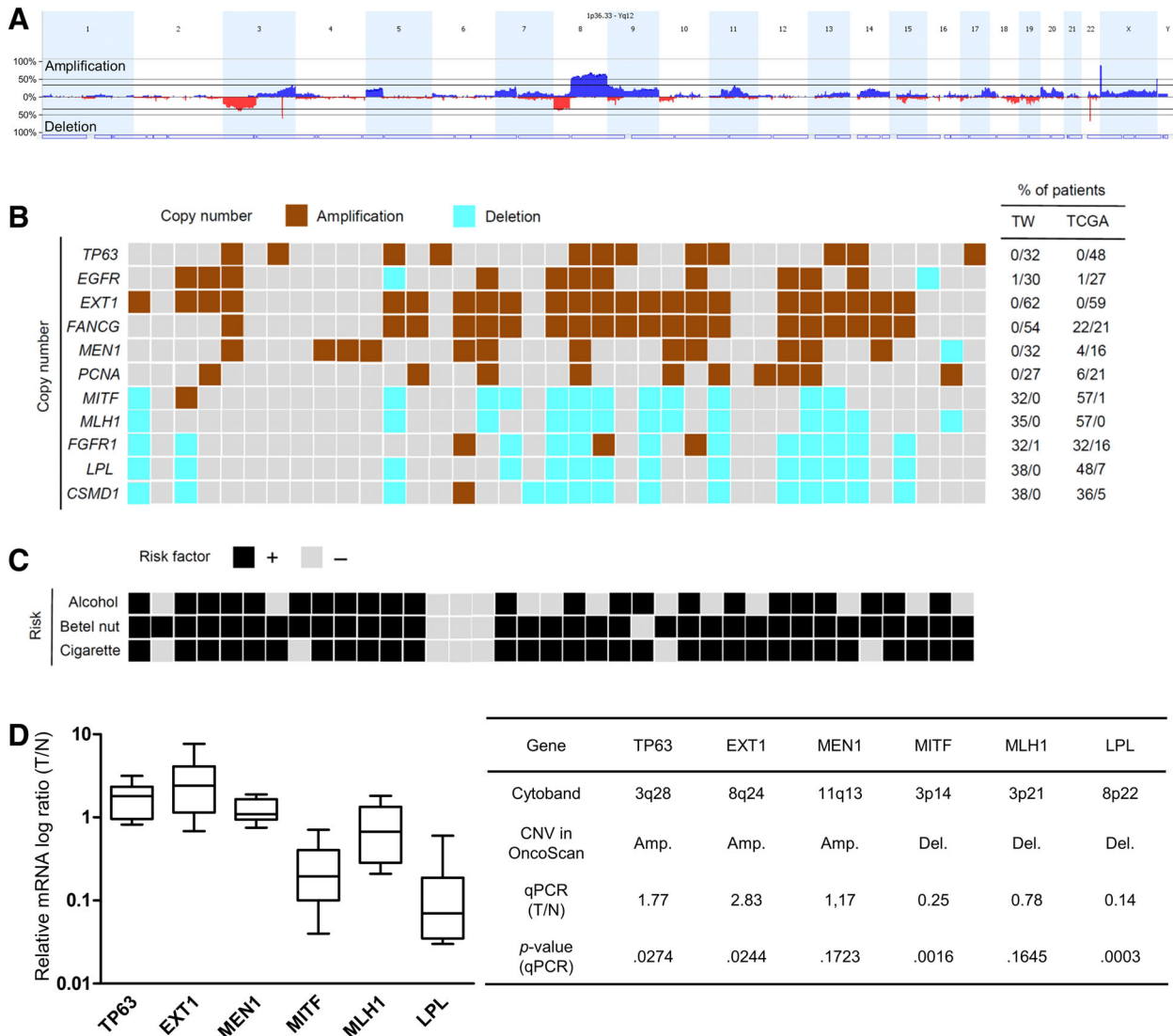
Figure 1. Summary data for the 37 cases of oral cavity squamous cell carcinoma (OSCC) in the Taiwan cohort. **(A):** Copy number profiling of 37 OSCC tissues in OncoScan assay. Blue color indicates copy number amplified regions, and red color indicates copy number deleted regions. The *y*-axis indicates the percentage of CNVs in 37 samples. **(B):** Heatmap representation of the copy number variations compared with those from TCGA. The table on the right shows the percentages of patients with the respective deletion or amplification, as found in the Taiwanese and TCGA OSCC cohorts. **(C):** Patients with OSCC with the habits of alcohol, betel nut, or cigarette use are individually marked. **(D):** Box-and-whisker plot showing the relative mRNA levels of 6 CNV genes determined in first testing cohort, including eight paired OSCC samples (left). Data are presented as the upper and lower quartiles and ranges (box), median values (horizontal line), and middle 90% distributions (dashed line). The table on the right shows the CNVs in OncoScan and T/N fold in qPCR. The *p* values were calculated by using paired *t* tests.
Abbreviations: Amp., amplification; CNV, copy number variation; Del., deletion; qPCR, quantitative polymerase chain reaction; T/N, tumor tissue sample and paired normal tissue sample; TCGA, The Cancer Genome Atlas; TW, Taiwan.

the genetic events involved in cancer development [35–38] that might result in up- or downregulation of mRNA expression in OSCC tumors.

Elevated MLLT3 Levels in Patients with OSCC Are Correlated with Poorer Prognosis

To identify novel genomic alterations for OSCC, we compared our data set with six genome-wide CNV data sets published previously for OSCC tumors in Asian populations (supplemental online Table 4). By this comparison, we found a novel copy number amplified region, chromosome 9p, encompassing genes including *PAX5, FANCG, MLLT3, RRAGA, PSIP1, JAK2,* and *NFIB.* The distribution of CNVs from OSCC-Taiwan cases in

chromosome 9 is presented in Figure 2A. Among these potential candidates, three have been previously reported as dysregulated proteins or genes in OSCC or HNSCC, including *PAX5, FANCG,* and *JAK2* [39–41]. Therefore, the other four candidates are potential novel dysregulated proteins or genes in OSCC. After reviewing the existent literature for the clinical relevance and molecular functions of these four candidates, we further chose to examine the association of MLLT3 with the clinicopathological manifestation in OSCC tumors. As shown in Figure 2B, we examined the mRNA expression of MLLT3 in second testing cohort, including 127 OSCC tissue specimens containing tumors and their corresponding normal tissues. We found that the mRNA levels of MLLT3 increased in OSCC tumors compared with those
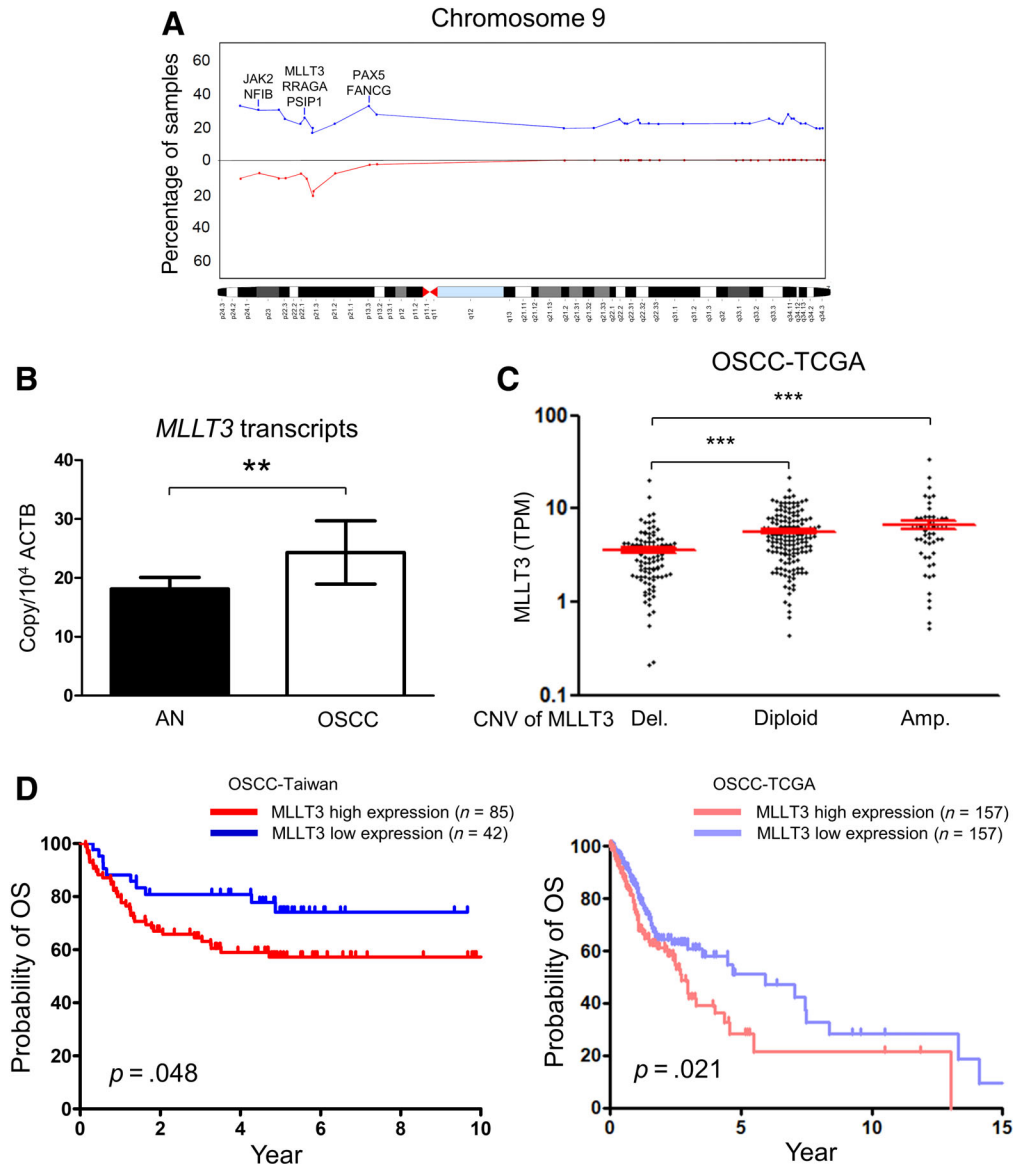
Figure 2. Association of high MLLT3 expression with poor prognosis of patient survival in oral cavity squamous cell carcinoma (OSCC). **(A):** The CNVs of OSCC-Taiwan cases in chromosome 9. Blue color indicates copy number amplifications, and red color indicates copy number deletions. The dots indicate the identified genes in the OncoScan array. **(B):** MLLT3 transcripts in 127 paired OSCC tissues were determined by quantitative polymerase chain reaction. **(C):** Positive correlation between the copy numbers of MLLT3 and its transcript expression levels in the OSCC-TCGA data set. The y-axis shows the MLLT3 TPM. The x-axis shows the copy number status of MLLT3. The red line indicates the mean ± SE of the MLLT3 transcripts. **(D):** Kaplan-Meier plot showing that the 5-year OS rates for patient subgroups stratified by high versus low MLLT3 expression were 58.8% and 76.2%, respectively ($p = .048$) in the OSCC-Taiwan data set (left). Kaplan-Meier plot for OS in subgroups stratified by MLLT3 expression among the 314 patients in the OSCC-TCGA data set ($p = .021$) (right). The p values were calculated by using log-rank tests. **$p < .01$, ***$p < .001$.
Abbreviations: ACTB, β-actin; Amp., amplification; AN, adjacent normal; CNV, copy number variation; Del., deletion; OS, overall survival; OSCC-Taiwain, data from Taiwanese patients with OSCC; OSCC-TCGA, OSCC data from TCGA; TCGA, The Cancer Genome Atlas; TPM, transcripts per million.

of their corresponding normal tissues. Furthermore, we also assessed and externally validated the relationship between MLLT3 transcript expression and genomic copy numbers by using the OSCC-TCGA data set. Notably, the MLLT3 transcript expression was positively correlated with its genomic copy number in 314 patients with OSCC in TCGA database (Fig. 2C). Clinicopathological analysis showed that the MLLT3 expression levels in OSCC tumors were positively associated with node classification and overall TNM stage ($p < .05$; Table 1), whereas there was no significant association between the MLLT3

expression level and other parameters such as sex, age, tumor classification, extranodal extension, and differentiation. Next, we utilized a survival analysis to evaluate the prognostic significance of MLLT3 in OSCC. The survival analysis revealed that patients with high MLLT3 expression exhibited poorer overall survival (OS) rates than those with low MLLT3 expression, and the 5-year OS rates for patients with high and low MLLT3 expression were 58.8% and 76.2%, respectively ($p = .048$; Fig. 2D). For external validation for this gene in the public domain, the data from 314 TCGA oral cancer samples

Table 1. Clinicopathological characteristics related to the expression of MLLT3 in 127 samples of oral cavity squamous cell carcinoma

| Patient categories | Case number | MLLT3 expression level, n (%) | | p value |
		Low	High	
Sex				
Male	115	37 (32.2)	78 (67.8)	.506
Female	12	5 (41.7)	7 (58.3)	
Age, years				
Mean ± SD		51.0 ± 14.2	51.4 ± 11.5	.866
Range		80.7–22.5	79.8–220.3	
Tumor classification				
T1–T2	64	25 (39.1)	39 (60.9)	.148
T3–T4	63	17 (27.0)	46 (73.0)	
Node classification				
0	65	29 (44.6)	36 (55.4)	.005[a]
>0	62	13 (21.0)	49 (79.0)	
Overall TNM stage				
I–II	39	20 (51.3)	19 (48.7)	.004[a]
III–IV	88	22 (25.0)	66 (75.0)	
ENE				
No	95	31 (32.6)	64 (67.4)	.856
Yes	32	11 (34.4)	21 (65.6)	
Differentiation				
Well + moderately	111	35 (31.5)	76 (68.5)	.331
Poorly	16	7 (43.7)	9 (56.3)	

[a]These are considered statistically significant.

Abbreviation: ENE, extranodal extension.

predominantly obtained from the U.S. were also analyzed, and the OS rates, as shown in Figure 2D, were also significantly different between high and low MLLT3 expression in the OSCC-TCGA data set (p = .021).

MLLT3 Is Involved in Cell Migration and Invasion Ability in OSCC Cells

The current study found that MLLT3 levels in OSCC were positively associated with node classification, overall TNM stage, and poorer prognosis, indicating that MLLT3 plays a vital role in regulation of cell motility and cancer invasiveness. Therefore, we adopted the siRNA approach to suppress the expression of endogenous MLLT3 in OC3 and OEC-M1 cells and assessed the effects on cell cycle, migration, and invasion. Figure 3A indicates that MLLT3 protein levels were significantly reduced in the cells transfected with MLLT3 siRNA compared with the cells transfected with control siRNA (p < .05). The flow cytometry assay revealed different effects on cell cycle for OSCC cells transfected with MLLT3 siRNA compared with the cells transfected with control siRNA. The MLLT3-knockdown OC3 cells revealed cell cycle arrest in G1 phase, but MLLT3-knockdown OEC-M1 cells displayed no changes (Fig. 3B). In addition, the Transwell migration assay showed that the migration ability of MLLT3-knockdown OC3 and OEC-M1 cells was decreased compared with that of the control cells (Fig. 3C). We further examined the invasion ability in MLLT3-knockdown cells. Figure 3D demonstrates that

the invasion ability was also significantly impaired in MLLT3-knockdown OC3 and OEC-M1 cells (p < .001). Collectively, these results indicate that MLLT3 is involved in OSCC cell migration and invasiveness.

CITED4 Plays an Opposite Role for MLLT3-Mediated Invasion Ability in OSCC

Previously, Li et al. performed ChIP experiments followed by high-throughput sequencing (ChIP-seq) to assess the chromatin occupancy of MLLT3. Compared with the non-repetitive genome background, they established 338 MLLT3-occupied genes (MLLT3 ChIP-seq data set) [42]. In addition, MLLT3-Dot1L complexes mediated transcriptional repression through hypermethylation of H3K79 at associated gene promoters, such as ENaCα and Tbr1 [19, 29]. Accordingly, we compared the MLLT3 ChIP-seq data set with the inversely correlated genes of MLLT3 in OSCC-TCGA. By this analysis, we identified three candidate genes (*CITED4*, *ID1*, and *S100P*) that might be transcriptionally repressed through MLLT3-Dot1L-associated hypermethylation at their promoter region (Fig. 4A). Among the three candidates, the expression of CITED4 showed a significantly inverse correlation with MLLT3 expression (Spearman's correlation coefficient, ρ = −0.316, p = 9.67E-8; Fig. 4B). To test this hypothesis, the mRNA expression of CITED4 was measured in MLLT3-knockdown OSCC cells. As shown in Figure 4C, the mRNA expression levels of CITED4 significantly increased in
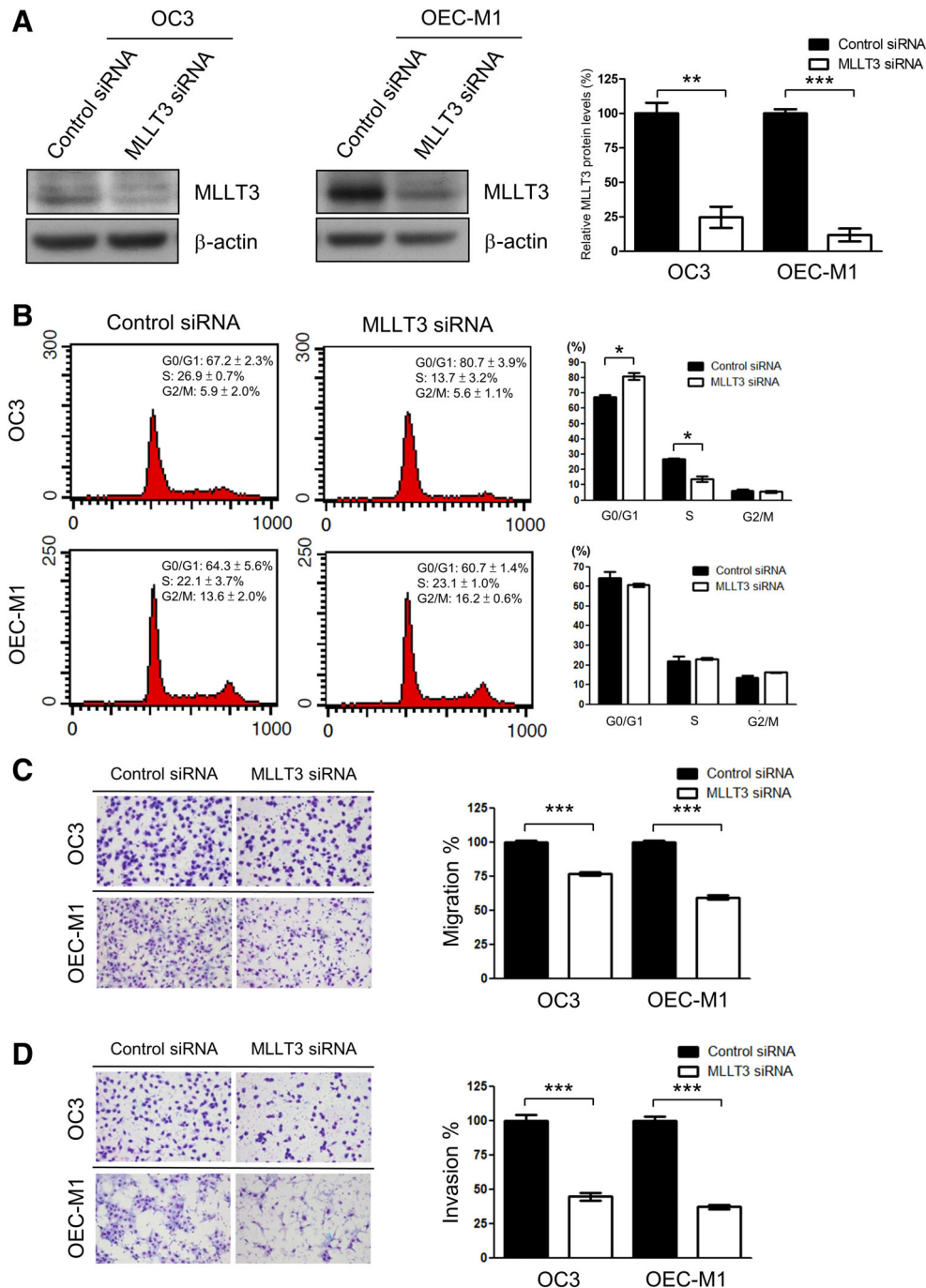
Figure 3. MLLT3 is involved in the migration and invasion ability of oral cavity squamous cell carcinoma cells. **(A):** OC3 and OEC-M1 cells were transfected with control siRNA and MLLT3-specific siRNA. MLLT3 protein expression was analyzed by Western blotting. β-actin was used as the loading control. Cells were simultaneously subjected to the following assays. The signal intensities were normalized to β-actin of these proteins and presented in a histogram. Data are presented as the mean values obtained from three independent experiments. Error bars indicate the SE. The *p* values were calculated by using the paired *t* test. **(B):** After transfection for 48 hours, DNA content was determined by propidium iodide staining followed by flow cytometry analysis. Quantification analysis of cell cycle distributions acquired from three independent experiments. The transfected cells were subjected to migration **(C)** and invasion **(D)** assays. Representative microphotographs of the filters obtained from the migration and invasion assays. Original magnification: ×100 (left). Quantitative analysis of the migration and invasion assays (right). Data are presented as the mean values obtained from three independent experiments. Error bars indicate the SE. The *p* values were calculated by using the Mann-Whitney *U* test. *$p < .05$, **$p < .01$, ***$p < .001$. Abbreviation: siRNA, small interfering RNA.

MLLT3-knockdown OC3 and OEC-M1 cells compared with those in control cells ($p < .001$). Consequently, to evaluate whether CITED4 plays a dominant role in MLLT3-regulated invasion ability in OSCC, we simultaneously suppressed the expression of MLLT3 and CITED4 and measured the difference in OSCC cell invasion. Western blotting revealed that both MLLT3 and CITED4 protein levels were significantly reduced in OEC-M1 cells transfected with MLLT3 or/and
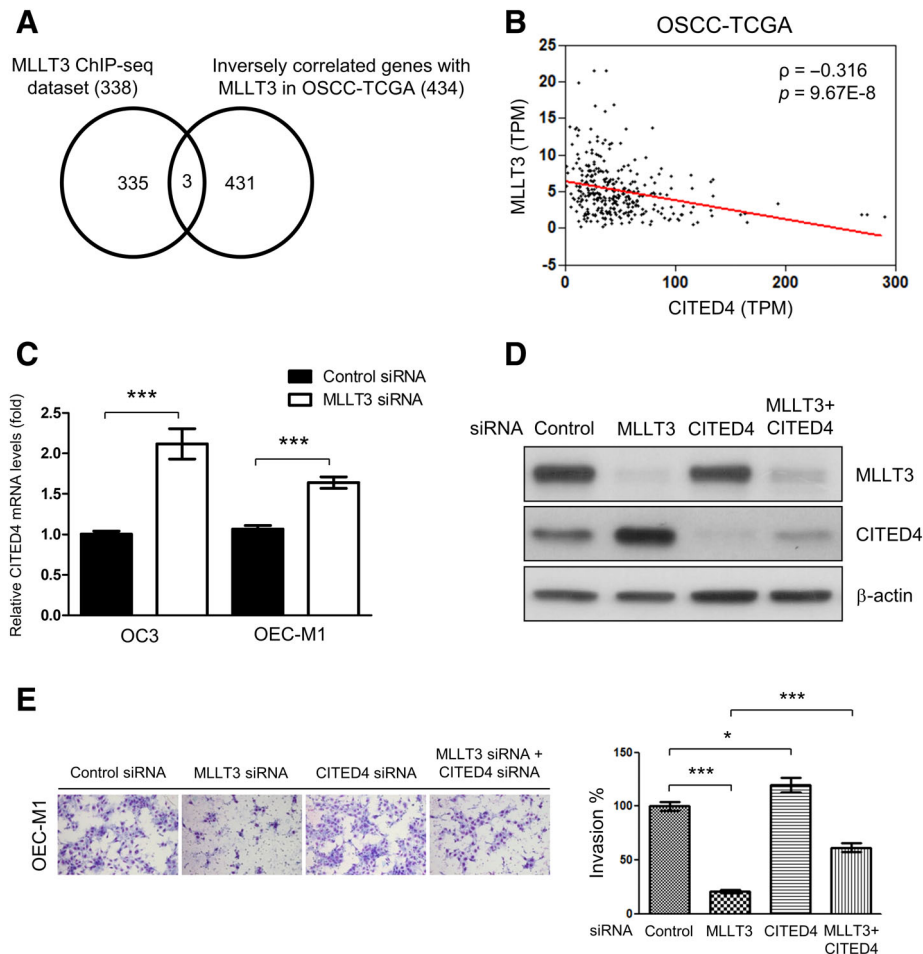
Figure 4. CITED4 plays an opposite role for MLLT3-mediated invasion ability in OSCC. **(A):** Comparison of the MLLT3 ChIP-seq data set with genes inversely correlated with MLLT3 in OSCC-TCGA. **(B):** A total of 315 unique OSCC samples, which have anatomic sites within the oral cavity and are classified as squamous cell carcinoma, were used in this analysis. Spearman's correlation between the expression levels of MLLT3 and all the other genes were calculated with Partek Genomics Suite software, followed by adjustment of the p value with the Benjamini-Hochberg method. Spearman's correlation coefficient (ρ) = -0.316; $p = 9.67E{-}8$. **(C):** Total RNA from OC3 or OEC-M1 cells transfected with control siRNA or MLLT3 siRNA was purified and reverse-transcribed, and the resulting cDNA was subjected to quantitative polymerase chain reaction analysis using CITED4 primers. **(D):** OEC-M1 cells were transfected with control siRNA, MLLT3, and CITED4-specific siRNA. MLLT3 and CITED4 protein expression was analyzed by Western blotting. β-actin was used as the loading control. Cells were simultaneously subjected to invasion assay **(E)**. Representative microphotographs of the filters obtained from the invasion assay. Original magnification: ×100 (left). Quantitative analysis of the invasion assay (right). Data are presented as the mean values obtained from three independent experiments. Error bars indicate the SE. The p values were calculated by using the Mann-Whitney U test. *p < .05, ***p < .001.

Abbreviations: ChIP-seq, chromatin immunoprecipitation followed by high-throughput sequencing; OSCC, oral cavity squamous cell carcinoma; OSCC-TCGA, OSCC data from TCGA; siRNA, small interfering RNA; TCGA, The Cancer Genome Atlas; TPM, transcripts per million.

CITED4 siRNA compared with the levels in cells transfected with control siRNA (Fig. 4D). The Transwell invasion assay demonstrated that the invasion ability showed an increase in CITED4-knockdown OEC-M1 cells. Notably, the invasion ability was significantly rescued in double knockdown of MLLT3 and CITED4 cells compared with that in MLLT3 knockdown cells (p < .001; Fig. 4E), suggesting that CITED4 plays a vital role in MLLT3-mediated invasion ability in OSCC.

Knockdown of MLLT3 Impairs Dot1L Associated with the CITED4 Promoter as a Consequence of HIF-1α-Mediated Gene Dysregulation in OSCC

MLLT3 interacts with the methyltransferase Dot1L, which mediates H3K79 methylation as a consequence of transcriptional repression for target genes. We next investigated whether the observed increase in CITED4 expression in MLLT3-knockdown OSCC cells occurred through modulating a change in Dot1L-associated hypermethylation at the CITED4 promoter. We performed ChIP with chromatin isolated from control and MLLT3 siRNA-transfected OEC-M1 cells and examined Dot1L with primers surrounding the TSS (+1) of the human *CITED4* gene via qPCR. As shown in Figure 5A, knockdown of MLLT3 led to a dramatic reduction in Dot1L at TSS on the *CITED4* gene. In addition, we also verified the Dot1L-chromatin complex with primers surrounding the TSS of the human *TCF4*, which had previously been found to be a Dot1L-associated gene [43]. We found that the levels of Dot1L at TSS on the *TCF4* gene were similar between control and MLLT3 siRNA-transfected OEC-M1 cells (Fig. 5A) Furthermore, when we measured the endogenous levels of Dot1L in
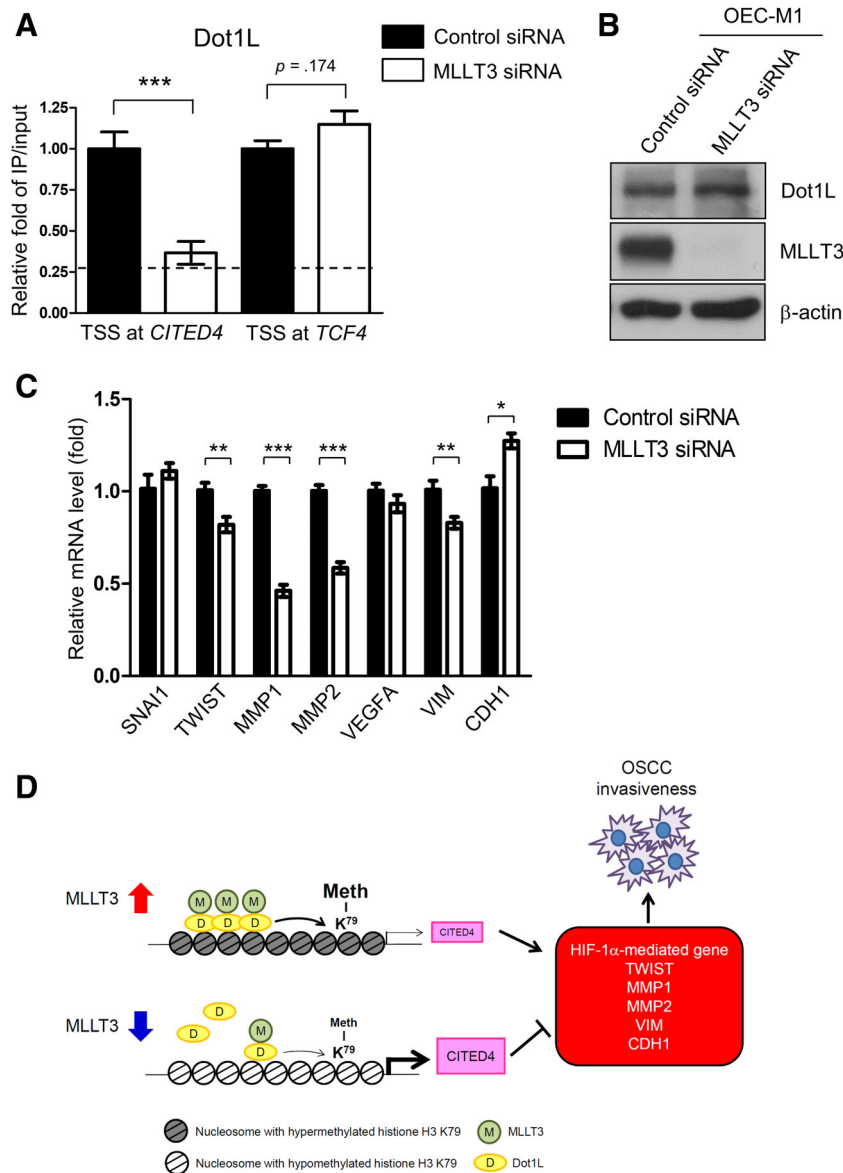
Figure 5. Knockdown of MLLT3 impairs Dot1L associated with the CITED4 promoter as a consequence of HIF-1α-mediated gene dysregulation in OSCC. **(A):** Chromatin immunoprecipitation of control and MLLT3 siRNA-transfected OEC-M1 cells. Antibodies used were IgG and anti-Dot1L. Precipitated DNA was assessed by quantitative polymerase chain reaction (qPCR) at the transcriptional start site on the *CITED4* and *TCF4* genes. Given is the amount of precipitated DNA relative to the respective input DNA $\pm$ SE of triplicates. The dotted line indicates the mean amplification of IgG control samples. **(B):** OEC-M1 cells were transfected with control siRNA and MLLT3-specific siRNA for 24 hours. Dot1L and MLLT3 protein expression were analyzed by Western blotting. β-actin was used as the loading control. **(C):** Total RNA from OEC-M1 cells transfected with control siRNA or MLLT3 siRNA was purified and reverse-transcribed, and the resulting cDNA was subjected to qPCR analysis using gene-specific primers. Data are presented as the mean values obtained from three independent experiments. Error bars indicate the SE. The *p* values were calculated by using the Mann-Whitney *U* test. **(D):** Hypothetical schematic of the role of MLLT3 in Dot1L-mediated transcriptional repression of CITED4 and OSCC invasiveness. In the OSCC cells, the elevated MLLT3 level triggered the Dot1L-mediated H3K79 hypermethylation at CITED4 promoter, which in turn suppressed the expression of CITED4, contributing to OSCC invasiveness. Under the repression of MLLT3 condition, the decreased MLLT3 level impaired the Dot1L-mediated H3K79 hypomethylation at the CITED4 promoter, followed by an elevation of CITED4, leading to dysregulation of HIF-1α-associated genes, as a consequence of inhibition for OSCC invasiveness. $*p < .05$, $**p < .01$, $***p < .001$.
Abbreviations: H3K79, histone H3 lysine 79; OSCC, oral cavity squamous cell carcinoma; siRNA, small interfering RNA; TSS, transcriptional start site.

MLLT3-knockdown OEC-M1 cells, the level of Dot1L was not reduced in MLLT3-knockdown OEC-M1 cells (Fig. 5B), suggesting that the reduction associated with the CITED4 promoter was not caused by downregulating Dot1L expression.

To test whether the HIF-1α-dependent expression of genes known to play a role in modulating tumor invasion and metastasis might be dysregulated in MLLT3-knockdown OSCC cells, the HIF-1α-mediated genes that modulate tumor

invasion or metastasis were analyzed by using the TRRUST version 2 database [44], a manually curated database that collects transcription factor-target regulatory relationships based on experimental observations rather than bioinformatics prediction. From this data set, we chose seven genes that had been well characterized as involved in cell invasion, migration, or epithelial-mesenchymal transition and measured the mRNA expression in MLLT3-knockdown cells. As shown in Figure 5C, the mRNA expression levels of *TWIST*, *MMP1*, *MMP2*, *VIM*, and *CDH1* were significantly dysregulated in MLLT3-knockdown OEC-M1 compared with those in control cells. However, the mRNA expression levels of *SNAI1* and *VEGFA* were similar in MLLT3-knockdown and control cells. Collectively, these data showed that MLLT3 was required for Dot1L-associated hypermethylation at TSS on the promoter of the *CITED4* gene, which in turn suppressed the expression of CITED4, as a consequence of OSCC invasiveness via regulation of HIF-1α-mediated genes.

DISCUSSION

This is the first study demonstrating the frequent CNVs of OSCC in a Taiwanese population using the OncoScan array on FFPE tumor samples. We further found that chromosome 9p is a novel copy number amplified region in OSCC, via comparison with previous studies [13]. The chromosome 9p encompassing genes, including *PAX5*, *FANCG*, *MLLT3*, *RRAGA*, *PSIP1*, *JAK2*, and *NFIB*, are a novel genomic amplified region for OSCC. Among these potential candidates, three were previously reported as dysregulated proteins or genes in OSCC or HNSCC. A significant increase in *PAX5* expression was observed in OSCC-derived cell lines compared with that in human normal oral keratinocytes [39]. *FANCG* was identified as an amplified gene in OSCC using array-based comparative genomic hybridization [40]. The inhibition of the *JAK2* signaling pathway could reduce tumor-induced angiogenesis by utilizing an HNSCC mouse model [41]. Accordingly, these results suggest that the findings in the current study are quite reproducible and feasible for discovery of the CNVs and dysregulated genes for OSCC tumors.

MLLT3 was shown to play important roles in cell proliferation, migration, and invasion via a microRNA silencing approach [45, 46]. Previously, downregulation of MLL-MLLT3 with antisense oligodeoxyribonucleotides decreased the expression of the *HOXA7* and *HOXA10* genes and induced apoptosis in a human leukemia cell line, THP-1 [47]. Furthermore, when the endogenous MLL-MLLT3 was suppressed via siRNA silencing in THP-1 cells, the comprehensive gene expression profile suggested several cellular processes (ribosomal biogenesis, chaperone binding, calcium homeostasis, and estrogen response) and 41 genes as likely mediators of MLL-MLLT3 leukemogenic effects. Among those, seven gene products (AHR, ATP2B2, DRD5, HIPK2, PARP8, ROR2, and TAS1R3) were selected as candidate drug targets. The functional relevance of one of these, the dopamine receptor DRD5, was confirmed as an antagonist that resulted in reduced leukemic cell characteristics of THP-1 cells [48]. However, the detailed molecular mechanisms of MLLT3-mediated cancer invasiveness remain to be clarified. To the best of our knowledge, no previous study has demonstrated any involvement of MLLT3

on OSCC tumors, along with the potential implications of its antagonists on the treatment; therefore, the current studies discovered a novel regulatory mechanism for OSCC invasiveness via MLLT3-mediated Dot1L-suppressed CITED4 transcription.

Disruptor of telomeric sequencing-1 (Dot1) was initially discovered in budding yeast for its essential role in the regulation of telomeric silencing [23]. Dot1 and its mammalian homolog, Dot1L, possess histone methyltranferase activity toward histone H3K79 [49], which regulates diverse cellular processes such as transcriptional regulation, cell cycle regulation, DNA damage response, differentiation, and development of leukemia [49–52]. Recently, several publications have reported that Dot1L plays a crucial role in leukemia as well as in solid tumors, such as breast cancer, esophageal squamous cell carcinoma, colorectal cancer, prostate cancer, gastric cancer, and ovarian cancer [53–58]. Furthermore, Dot1L is a drug target for mixed-lineage leukemia (MLL) gene-rearranged leukemia [27, 59, 60]. Several Dot1L inhibitors have shown effective suppression of proliferation, migration, and invasion in ovarian cancer and breast cancer [58, 61]. However, in the current literature, the role of Dot1L on OSCC tumorigenesis and progression has not yet been investigated. The current study provides the first evidence for the potential involvement of its association with OSCC tumors and might further indicate these prospective targets for OSCC therapy in the future.

CITED4 belongs to the CITED family, members of which have critical roles during cell development [62, 63]. CITED4 interacts with CBP/p300, as well as the transcription factor AP-2 (TFAP2), mediating TFAP2-dependent transcription [62]. Notably, CITED4 is downregulated in several cancer types, including colorectal cancer, brain cancer, and breast cancer, and contributes to the acquisition of malignant characteristics such as proliferation, survival, angiogenesis, and adherens junctions/tight junctions [64–66]. Furthermore, Fox et al. showed that the expression of CITED4 can be downregulated or translocated to the cytoplasm in breast cancer and inhibits HIF-1α-mediated transcription and angiogenesis through direct competition of p300 binding. Analysis of CITED4 in a large series of human breast tumors by immunohistochemistry showed both cytoplasmic and nuclear staining; the nuclear staining of CITED4 negatively correlated with HIF-1α expression, tumor size, and tumor grade [66]. In addition, several studies have recently shown that HIF-1α expression plays a role in OSCC tumorigenesis, facilitating the adaptation of cells to hypoxia as well as contributing to the invasive properties, cell survival, and angiogenesis in these tumors [67–69]. In the current study, MLLT3 was further confirmed to be required for HIF-1α-mediated gene transcription, such as *TWIST*, *MMP1*, *MMP2*, *VIM*, and *CDH1*. Notably, the mRNA expression level of *TWIST* indicated that it promotes OSCC cell invasion and is associated with poor survival in OSCC [70, 71]. An increased *MMP1* expression level was detected in patients with OSCC compared with that in healthy controls and was related to metastasis [72–74]. The expression levels of *MMP2* were notably elevated in the metastatic regions of OSCC compared with those in the primary region [75]. The epithelial-mesenchymal transition related molecules, *VIM* and *CDH1*, were significantly associated with lymph node metastasis and patient survival in OSCC [76–78]. Taken together, these results indicate that MLLT3 might play a pivotal role in OSCC invasiveness.

Conclusion

The current study demonstrates, for the first time in the literature, that knockdown of MLLT3 significantly increased the expression of CITED4 via suppressing the Dot1L associated with TSS on *CITED4*, followed by dysregulation of HIF-1α-dependent expression of genes such as *TWIST*, *MMP1*, *MMP2*, *VIM*, and *CDH1*, suggesting that MLLT3 could be one of the fundamental factors in OSCC invasiveness (Fig. 5D). Accordingly, the current study elucidated the clinicopathological associations and molecular mechanisms of a novel marker, MLLT3, in OSCC carcinogenesis.

Author Contributions

Chun-I Wang, Huang-Kai Kao, Ting-Wen Chen, Yenlin Huang, Hsing-Wen Cheng, Jui-Shan Yi, Shao-Yu Hung, Chi-Sheng Wu, Yun-Shien Lee, Kai-Ping Chang
Conception/design: Chun-I Wang, Huang-Kai Kao, Kai-Ping Chang
Provision of study material or patients: Yenlin Huang, Kai-Ping Chang
Collection and/or assembly of data: Chun-I Wang, Huang-Kai Kao, Ting-Wen Chen, Hsing-Wen Cheng, Jui-Shan Yi, Shao-Yu Hung
Data analysis and interpretation: Chun-I Wang, Huang-Kai Kao, Ting-Wen Chen, Yenlin Huang, Chi-Sheng Wu, Yun-Shien Lee
Manuscript writing: Chun-I Wang, Huang-Kai Kao
Final approval of manuscript: Chun-I Wang, Huang-Kai Kao, Ting-Wen Chen, Yenlin Huang, Hsing-Wen Cheng, Jui-Shan Yi, Shao-Yu Hung, Chi-Sheng Wu, Yun-Shien Lee, Kai-Ping Chang

References

1. Siegel R, Naishadham D, Jemal A. Cancer statistics, 2013. CA Cancer J Clin 2013;63:11–30.

2. Jemal A, Bray F, Center MM et al. Global cancer statistics. CA Cancer J Clin 2011;61:69–90.

3. Wang CI, Yu CJ, Huang Y et al. Association of overexpressed karyopherin alpha 2 with poor survival and its contribution to interleukin-1β-induced matrix metalloproteinase expression in oral cancer. Head Neck 2018;40:1719–1733.

4. De Paz D, Kao HK, Huang Y et al. Prognostic stratification of patients with advanced oral cavity squamous cell carcinoma. Curr Oncol Rep 2017;19:65.

5. Ponder BA. Genetic predisposition to cancer. Br J Cancer 1991;64:203–204.

6. Ranadive KJ, Ranadive SN, Shivapurkar NM et al. Betel quid chewing and oral cancer: Experimental studies on hamsters. Int J Cancer 1979;24:835–843.

7. Degawa M, Stern SJ, Martin MV et al. Metabolic activation and carcinogen-DNA adduct detection in human larynx. Cancer Res 1994;54:4915–4919.

8. Reshmi SC, Gollin SM. Chromosomal instability in oral cancer cells. J Dent Res 2005;84:107–117.

9. Viet CT, Schmidt BL. Understanding oral cancer in the genome era. Head Neck 2010;32:1246–1268.

10. Califano J, van der Riet P, Westra W et al. Genetic progression model for head and neck cancer: Implications for field cancerization. Cancer Res 1996;56:2488–2492.

11. Pinkel D, Segraves R, Sudar D et al. High resolution analysis of DNA copy number variation using comparative genomic hybridization to microarrays. Nat Genet 1998;20:207–211.

12. Hanahan D, Weinberg RA. Hallmarks of cancer: The next generation. Cell 2011;144:646–674.

13. Salahshourifar I, Vincent-Chong VK, Kallarakkal TG et al. Genomic DNA copy number alterations from precursor oral lesions to oral squamous cell carcinoma. Oral Oncol 2014;50:404–412.

14. Foster JM, Oumie A, Togneri FS et al. Cross-laboratory validation of the OncoScan FFPE assay, a multiplex tool for whole genome tumour profiling. BMC Med Genomics 2015;8:5.

15. Chen W, Kumar AR, Hudson WA et al. Malignant transformation initiated by MLL-AF9: Gene dosage and critical target cells. Cancer Cell 2008;13:432–440.

16. Lin JJ, Hemenway CS. Hsp90 directly modulates the spatial distribution of AF9/MLLT3 and affects target gene expression. J Biol Chem 2010;285:11966–11973.

17. Erfurth F, Hemenway CS, de Erkenez AC et al. MLL fusion partners AF4 and AF9 interact at subnuclear foci. Leukemia 2004;18:92–102.

18. Hemenway CS, de Erkenez AC, Gould GC. The polycomb protein MPc3 interacts with AF9, an MLL fusion partner in t(9;11)(p22;q23) acute leukemias. Oncogene 2001;20:3798–3805.

19. Zhang W, Xia X, Reisenauer MR et al. Dot1a-AF9 complex mediates histone H3 Lys-79 hypermethylation and repression of ENaCalpha in an aldosterone-sensitive manner. J Biol Chem 2006;281:18059–18068.

20. Bitoun E, Oliver PL, Davies KE. The mixed-lineage leukemia fusion partner AF4 stimulates RNA polymerase II transcriptional elongation and mediates coordinated chromatin remodeling. Hum Mol Genet 2007;16:92–106.

21. Ng HH, Feng Q, Wang H et al. Lysine methylation within the globular domain of histone H3 by Dot1 is important for telomeric silencing and Sir protein association. Genes Dev 2002;16:1518–1527.

22. Feng Q, Wang H, Ng HH et al. Methylation of H3-lysine 79 is mediated by a new family of HMTases without a SET domain. Curr Biol 2002;12:1052–1058.

23. van Leeuwen F, Gafken PR, Gottschling DE. Dot1p modulates silencing in yeast by methylation of the nucleosome core. Cell 2002;109:745–756.

24. Bostelman LJ, Keller AM, Albrecht AM et al. Methylation of histone H3 lysine-79 by Dot1p plays multiple roles in the response to UV damage in *Saccharomyces cerevisiae*. DNA Repair (Amst) 2007;6:383–395.

25. Shanower GA, Muller M, Blanton JL et al. Characterization of the grappa gene, the Drosophila histone H3 lysine 79 methyltransferase. Genetics 2005;169:173–184.

26. Steger DJ, Lefterova MI, Ying L et al. DOT1L/KMT4 recruitment and H3K79 methylation are ubiquitously coupled with gene transcription in mammalian cells. Mol Cell Biol 2008;28:2825–2839.

27. Okada Y, Feng Q, Lin Y et al. hDOT1L links histone methylation to leukemogenesis. Cell 2005;121:167–178.

28. Gazin C, Wajapeyee N, Gobeil S et al. An elaborate pathway required for Ras-mediated epigenetic silencing. Nature 2007;449:1073–1077.

29. Buttner N, Johnsen SA, Kugler S et al. Af9/Mllt3 interferes with Tbr1 expression through epigenetic modification of histone H3K79 during development of the cerebral cortex. Proc Natl Acad Sci USA 2010;107:7042–7047.

30. Srinivasan RS, de Erkenez AC, Hemenway CS. The mixed lineage leukemia fusion partner AF9 binds specific isoforms of the BCL-6 corepressor. Oncogene 2003;22:3395–3406.

31. Ji H, Kumm J, Zhang M et al. Molecular inversion probe analysis of gene copy alterations reveals distinct categories of colorectal carcinoma. Cancer Res 2006;66:7910–7919.

32. Wang Y, Carlton VE, Karlin-Neumann G et al. High quality copy number and genotype data from FFPE samples using Molecular Inversion Probe (MIP) microarrays. BMC Med Genomics 2009;2:8.

33. Chen TW, Lee CC, Liu H et al. APOBEC3A is an oral cancer prognostic biomarker in Taiwanese carriers of an APOBEC deletion polymorphism. Nat Commun 2017;8:465.

34. Cancer Genome Atlas Network. Comprehensive genomic characterization of head and neck squamous cell carcinomas. Nature 2015;517:576–582.

35. Pollack JR, Sorlie T, Perou CM et al. Microarray analysis reveals a major direct role of DNA copy number alteration in the transcriptional program of human breast tumors. Proc Natl Acad Sci USA 2002;99:12963–12968.

36. Orntoft TF, Thykjaer T, Waldman FM et al. Genome-wide study of gene copy numbers, transcripts, and protein levels in pairs of non-invasive and invasive human transitional cell carcinomas. Mol Cell Proteomics 2002;1:37–45.

37. Yang S, Jeung HC, Jeong HJ et al. Identification of genes with correlated patterns of variations in DNA copy number and gene expression level in gastric cancer. Genomics 2007;89:451–459.

38. Zhang B, Wang J, Wang X et al. Proteogenomic characterization of human colon and rectal cancer. Nature 2014;513:382–387.

39. Norhany S, Kouzu Y, Uzawa K et al. Overexpression of PAX5 in oral carcinogenesis. Oncol Rep 2006;16:1003–1008.

40. Sparano A, Quesnelle KM, Kumar MS et al. Genome-wide profiling of oral squamous cell carcinoma by array-based comparative genomic hybridization. Laryngoscope 2006;116:735–741.

41. Liu JF, Deng WW, Chen L et al. Inhibition of JAK2/STAT3 reduces tumor-induced angiogenesis and myeloid-derived suppressor cells in head and neck cancer. Mol Carcinog 2018;57:429–439.

42. Li Y, Wen H, Xi Y et al. AF9 YEATS domain links histone acetylation to DOT1L-mediated H3K79 methylation. Cell 2014;159:558–571.

43. Mahmoudi T, Boj SF, Hatzis P et al. The leukemia-associated Mllt10/Af10-Dot1l are Tcf4/β-catenin coactivators essential for intestinal homeostasis. PLoS Biol 2010;8:e1000539.

44. Han H, Cho JW, Lee S et al. TRRUST v2: An expanded reference database of human and mouse transcriptional regulatory interactions. Nucleic Acids Res 2018;46:D380–D386.

45. Meng FJ, Meng FM, Wu HX et al. miR-564 inhibited metastasis and proliferation of prostate cancer by targeting MLLT3. Eur Rev Med Pharmacol Sci 2017;21:4828–4834.

46. Zhang T, Luo Y, Wang T et al. MicroRNA-297b-5p/3p target Mllt3/Af9 to suppress lymphoma cell proliferation, migration and invasion in vitro and tumor growth in nude mice. Leuk Lymphoma 2012;53:2033–2040.

47. Kawagoe H, Kawagoe R, Sano K. Targeted down-regulation of MLL-AF9 with antisense oligodeoxyribonucleotide reduces the expression of the HOXA7 and -A10 genes and induces apoptosis in a human leukemia cell line, THP-1. Leukemia 2001;15:1743–1749.

48. Fleischmann KK, Pagel P, Schmid I et al. RNAi-mediated silencing of MLL-AF9 reveals leukemia-associated downstream targets and processes. Mol Cancer 2014;13:27.

49. Nguyen AT, Zhang Y. The diverse functions of Dot1 and H3K79 methylation. Genes Dev 2011;25:1345–1358.

50. Onder TT, Kara N, Cherry A et al. Chromatin-modifying enzymes as modulators of reprogramming. Nature 2012;483:598–602.

51. McLean CM, Karemaker ID, van Leeuwen F. The emerging roles of DOT1L in leukemia and normal development. Leukemia 2014;28:2131–2138.

52. Wakeman TP, Wang Q, Feng J et al. Bat3 facilitates H3K79 dimethylation by DOT1L and promotes DNA damage-induced 53BP1 foci at G1/G2 cell-cycle phases. EMBO J 2012;31:2169–2181.

53. Cho MH, Park JH, Choi HJ et al. DOT1L cooperates with the c-Myc-p300 complex to epigenetically derepress CDH1 transcription factors in breast cancer progression. Nat Commun 2015;6:7821.

54. Singh V, Singh LC, Singh AP et al. Status of epigenetic chromatin modification enzymes and esophageal squamous cell carcinoma risk in northeast Indian population. Am J Cancer Res 2015;5:979–999.

55. Kryczek I, Lin Y, Nagarsheth N et al. IL-22(+) CD4(+) t cells promote colorectal cancer stemness via STAT3 transcription factor activation and induction of the methyltransferase DOT1L. Immunity 2014;40:772–784.

56. Annala M, Kivinummi K, Leinonen K et al. DOT1L-HES6 fusion drives androgen independent growth in prostate cancer. EMBO Mol Med 2014;6:1121–1123.

57. Donner I, Kiviluoto T, Ristimaki A et al. Exome sequencing reveals three novel candidate predisposition genes for diffuse gastric cancer. Fam Cancer 2015;14:241–246.

58. Zhang X, Liu D, Li M et al. Prognostic and therapeutic value of disruptor of telomeric silencing-1-like (DOT1L) expression in patients with ovarian cancer. J Hematol Oncol 2017;10:29.

59. Krivtsov AV, Feng Z, Lemieux ME et al. H3K79 methylation profiles define murine and human MLL-AF4 leukemias. Cancer Cell 2008;14:355–368.

60. Daigle SR, Olhava EJ, Therkelsen CA et al. Selective killing of mixed lineage leukemia cells by a potent small-molecule DOT1L inhibitor. Cancer Cell 2011;20:53–65.

61. Zhang L, Deng L, Chen F et al. Inhibition of histone H3K79 methylation selectively inhibits proliferation, self-renewal and metastatic potential of breast cancer. Oncotarget 2014;5:10665–10677.

62. Braganca J, Swingler T, Marques FI et al. Human CREB-binding protein/p300-interacting transactivator with ED-rich tail (CITED) 4, a new member of the CITED family, functions as a co-activator for transcription factor AP-2. J Biol Chem 2002;277:8559–8565.

63. Yahata T, Takedatsu H, Dunwoodie SL et al. Cloning of mouse Cited4, a member of the CITED family p300/CBP-binding transcriptional coactivators: Induced expression in mammary epithelial cells. Genomics 2002;80:601–613.

64. Tews B, Roerig P, Hartmann C et al. Hypermethylation and transcriptional down-regulation of the CITED4 gene at 1p34.2 in oligodendroglial tumours with allelic losses on 1p and 19q. Oncogene 2007;26:5010–5016.

65. Rogers MA, Kalter V, Marcias G et al. CITED4 gene silencing in colorectal cancer cells modulates adherens/tight junction gene expression and reduces cell proliferation. J Cancer Res Clin Oncol 2016;142:225–237.

66. Fox SB, Braganca J, Turley H et al. CITED4 inhibits hypoxia-activated transcription in cancer cells, and its cytoplasmic location in breast cancer is associated with elevated expression of tumor cell hypoxia-inducible factor 1alpha. Cancer Res 2004;64:6075–6081.

67. Bhaijee F, Pepper DJ, Pitman KT et al. Cancer stem cells in head and neck squamous cell carcinoma: A review of current knowledge and future applications. Head Neck 2012;34:894–899.

68. Gilkes DM, Semenza GL, Wirtz D. Hypoxia and the extracellular matrix: Drivers of tumour metastasis. Nat Rev Cancer 2014;14:430–439.

69. De Lima PO, Jorge CC, Oliveira DT et al. Hypoxic condition and prognosis in oral squamous cell carcinoma. Anticancer Res 2014;34:605–612.

70. Kong YH, Syed Zanaruddin SN, Lau SH et al. Co-expression of TWIST1 and ZEB2 in oral squamous cell carcinoma is associated with poor survival. PLoS One 2015;10:e0134045.

71. Duan Y, He Q, Yue K et al. Hypoxia induced Bcl-2/Twist1 complex promotes tumor cell invasion in oral squamous cell carcinoma. Oncotarget 2017;8:7729–7739.

72. Yen CY, Chen CH, Chang CH et al. Matrix metalloproteinases (MMP) 1 and MMP10 but not MMP12 are potential oral cancer markers. Biomarkers 2009;14:244–249.

73. Yu JS, Chen YT, Chiang WF et al. Saliva protein biomarkers to detect oral squamous cell carcinoma in a high-risk population in Taiwan. Proc Natl Acad Sci USA 2016;113:11549–11554.

74. Tanis T, Cincin ZB, Gokcen-Rohlig B et al. The role of components of the extracellular matrix and inflammation on oral squamous cell carcinoma metastasis. Arch Oral Biol 2014;59:1155–1163.

75. Nishio K, Motozawa K, Omagari D et al. Comparison of MMP2 and MMP9 expression levels between primary and metastatic regions of oral squamous cell carcinoma. J Oral Sci 2016;58:59–65.

76. Fan CC, Wang TY, Cheng YA et al. Expression of E-cadherin, Twist, and p53 and their prognostic value in patients with oral squamous cell carcinoma. J Cancer Res Clin Oncol 2013;139:1735–1744.

77. Zhou J, Tao D, Xu Q et al. Expression of e-cadherin and vimentin in oral squamous cell carcinoma. Int J Clin Exp Pathol 2015;8:3150–3154.

78. Liu S, Liu L, Ye W et al. High vimentin expression associated with lymph node metastasis and predicated a poor prognosis in oral squamous cell carcinoma. Sci Rep 2016;6:38834.

See http://www.TheOncologist.com for supplemental material available online.